# Off-axis digital hologram reconstruction: some practical considerations

Nicolas Verrier* and Michael Atlan

Centre National de la Recherche Scientifique (CNRS), UMR 7587—Institut Langevin, Institut National de la Santé et de la Recherche Médicale (INSERM) U 979, Université Pierre et Marie Curie (UPMC), Université Paris 7, École Supérieure de Physique et de Chimie Industrielles (ESPCI ParisTech), 10 rue Vauquelin, 75005 Paris, France

*Corresponding author: nicolas.verrier@espci.fr

Received 1 August 2011; revised 19 September 2011; accepted 10 October 2011; posted 14 October 2011 (Doc. ID 152132); published 17 November 2011

Holographic rendering of off-axis intensity digital holograms is discussed. A review of some of the main numerical processing methods, based either on the Fourier transform interpretation of the propagation integral or on its linear system counterpart, is reported. Less common methods such as adjustable magnification reconstruction schemes and Fresnelet decomposition are presented and applied to the digital treatment of off-axis holograms. The influence of experimental parameters on the classical hologram reconstruction methods is assessed, offering guidelines for optimal image rendering regarding the hologram recording conditions. © 2011 Optical Society of America

*OCIS codes:* 090.1995, 100.3010.

## 1. Introduction

Optical holography consists of the acquisition of images from diffracted optical field measurements. Holographic imaging was initially proposed by Gabor [1] for electron microscopy. Holograms were recorded on high-resolution photographic plates. Because of the subsequently named "in-line" configuration, holograms were stained with twin-image and zero-order contributions, which overlapped with the signal image [2]. Originally recorded with the red radiation of mercury lamps, holograms were increasingly recorded with laser light sources, which gave much more reliable results. In 1962, Leith and Upatnieks proposed the introduction of an off-axis reference beam [3] to separate, in the spatial frequency domain, the real image from the twin-image and zero-order diffraction terms. However, holograms were still to be reconstructed by optical means.

The first digital reconstructions of optically measured holograms were realized by Goodman and Lawrence [4], and further by Kronrod *et al.* [5] (in Russian; more details can be found in Ref. [6]) in the early 1970s. Here, optically magnified parts of the holograms are digitally sampled and then reconstructed using Fourier transform based routines. Digitalization of optical holograms allowed, for instance, improvement of reconstruction quality [7], retrieval of information about the phase of the recording wave [8,9], and treatment of holograms without reconstruction [10]. One of the major breakthroughs in holographic imaging was initiated, by Schnars and Jüptner, with direct recording of digital holograms [11]. CCD and complementary metal oxide semiconductor (CMOS) digital sensor arrays enabled the acquisition and numerical processing of high-resolution holograms at fast rates.

Intrinsic properties of holographic imaging allow this technique to be used in a wide range of domains, such as fluid mechanics [12–20], biomedical imaging [21–26], and mechanical vibration analysis [27–35]. Democratization of high-resolution CCD and CMOS sensors played a major role in the development of

0003-6935/11/34H136-11$15.00/0

digital reconstruction techniques. For instance, reconstruction of phase-only [36], shifted [37], tilted, or aberrated data [38–40] has been successfully demonstrated. Inverse-problem approaches make it possible to improve object localization and field of view in the reconstructed hologram [41,42]. Compressive sensing based approaches are also to be considered when working in noisy or low-light conditions [43,44]. Moreover, due to the massive parallelization of image processing calculations by graphics processing units (GPUs), hologram reconstruction can be performed in real time [45–48].

In this paper, we will describe most of the common off-axis digital holographic reconstruction schemes and discuss their applicability. After some brief reminders about digital holographic recording, we will present the main reconstruction approaches, involving one to three Fourier transforms. Then a discussion about reconstruction with adjustable magnification is proposed. Methods to tackle aliases and replicas are proposed, leading to high-quality magnified reconstructions. The use of Fresnelet transform will also be discussed. Reconstruction methods will be assessed experimentally with optically acquired off-axis holograms, to provide insight into their respective suitability toward targeted applications.

## 2. Fresnel Holography Bases

Digital holography typically consists of recording an optical field emerging from an illuminated object in a diffraction plane (e.g., in free-space propagation conditions) and numerically calculating, from diffraction models, the field distribution in the reconstruction plane. In practice, optical holograms are measured out from the interference of the diffracted beam beating against a reference beam, which is not disturbed by the object to be analyzed. One of the object-reference cross terms typically yields a complex-valued map (i.e., quadrature-resolved—in amplitude and phase) of the diffraction field in the sensor plane. The complex-valued measurement contains relevant information about the local retardation of the diffracted field. Phase-shifting [49] and frequency-shifting [50] techniques were proposed to record the diffraction field in quadrature. The interference pattern, recorded by sensor array, can be expressed as [51]

$$E(x,y) = |\mathcal{R}(x,y)|^2 + |\mathcal{O}(x,y)|^2 + \mathcal{O}^*(x,y)\mathcal{R}(x,y) + \mathcal{O}(x,y)\mathcal{R}^*(x,y), \quad (1)$$

where $\mathcal{R}$ and $\mathcal{O}$ denote reference and object optical fields, respectively. Starred $(*)$ symbols are associated with complex conjugate values.

The interference between reference and object beams can be recorded within a wide range of configurations. These can be grouped in two main categories: in-line [51] and off-axis configurations [52]. For our applications, off-axis holograms will be recorded with a Mach–Zehnder configuration. The final part of our off-axis Mach–Zehnder configuration is illustrated in Fig. 1(a). Here, the reference and object beam are combined, with a relative angle $\alpha$, using a nonpolarizing beam-splitting/combining cube. It should be noted that $\alpha$ should be chosen so as to fulfill the sampling theorem. The maximal value leading to a correct sampling of the interference pattern is therefore given, under paraxial conditions, by

$$\alpha_{\max} \approx \frac{\lambda}{2\Delta x}, \quad (2)$$

where $\Delta x$ denotes the sampling rate of the recording device.

This off-axis angle results in separation of the four terms of Eq. (1) in the spatial frequency domain. This aspect is proposed Fig. 1(b). The central part of the hologram spectrum $(|\mathcal{R}(x,y)|^2 + |\mathcal{O}(x,y)|^2)$ is known as the autocorrelation term; its size is associated with the highest spatial frequencies of the object, denoted by $B$. Real and twin images of the object are respectively given by $\mathcal{O}\mathcal{R}^*$ and $\mathcal{R}\mathcal{O}^*$. These two terms are twice as small as the autocorrelation term. To improve the reconstruction quality, autocorrelation and twin-image terms have to be canceled. This can be achieved either by spatial filtering [53] or phase shifting [54]. Doing this makes it possible to reconstruct the real image term only.

In the next part, we will focus on hologram reconstruction. After a brief reminder about the Fresnel transform, we will discuss its main digital implementations.

## 3. Digital Hologram Reconstruction

Digital reconstruction of an hologram consists in *a posteriori* refocusing over the original object, which can be performed by calculating backward propagation of the light from the hologram to the reconstruction plane. This process is equivalent to positioning the recorded hologram back into the reference beam. The eference beam therefore becomes the reconstruction beam. Using the Huygens–Fresnel principle, one can infer an integral formulation of the intensity $E_{\text{rec}}$ in the reconstruction plane, from an off-axis

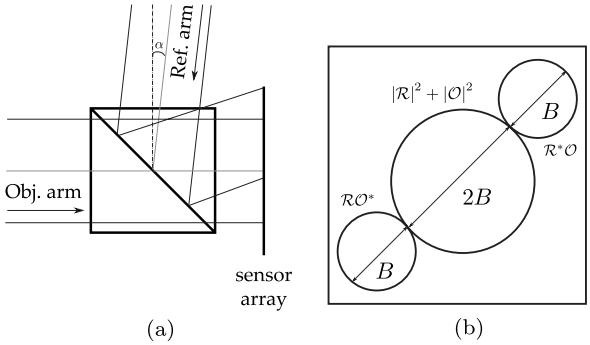


Fig. 1. (a) Hologram recording in off-axis configuration, (b) spatial frequency representation of off-axis holograms.

recorded hologram $E$ [55]:

$$E_{\mathrm{rec}}(\xi,\eta) = -i\frac{z}{\lambda}\int_{\mathbb{R}^2} E(x,y)\frac{\exp(ikr)}{r}\mathrm{d}x\mathrm{d}y. \quad (3)$$

Here, the distance $r$ is given by

$$r = \sqrt{z^2 + (x-\xi)^2 + (y-\eta)^2}, \quad (4)$$

where $(x,y)$ and $(\xi,\eta)$ denote the spatial coordinates in the hologram and reconstruction plane, respectively. It should be noted that the hologram $E(x,y)$ has been recorded as an off-axis configuration. Under Fresnel approximation, when $z^3 \gg \frac{1}{8\lambda}[(\xi-x)^2+(\eta-y)^2]^2$, $r$ can be approximated by

$$r = z\left[1 + \frac{1}{2}\left(\frac{x-\xi}{z}\right)^2 + \frac{1}{2}\left(\frac{y-\eta}{z}\right)^2\right], \quad (5)$$

and Eq. (3) is rewritten as

$$E_{\mathrm{rec}}(\xi,\eta) = \frac{\exp\left(\frac{i2\pi}{\lambda}z\right)}{i\lambda z}\int_{\mathbb{R}^2} E(x,y) \times \exp\left\{i\frac{\pi}{\lambda z}[(x-\xi)^2 + (y-\eta)^2]\right\}\mathrm{d}x\mathrm{d}y. \quad (6)$$

This relationship will be used in the remainder of this paper to perform reconstruction of off-axis intensity holograms.

As far as variables in Eq. (6) are separable, all the discrete formulations will be derived in the one-dimensional (1D) case. Generalization in two dimensions is straightforward. The 1D discrete Fresnel transform is defined by

$$E_{\mathrm{rec}}(p) = \frac{\exp\left(\frac{i2\pi}{\lambda}z\right)}{i\lambda z}\exp\left(i\frac{\pi}{\lambda z}p^2\Delta\xi^2\right)\sum_{n=0}^{N-1}E(n) \times \exp\left(i\frac{\pi}{\lambda z}n^2\Delta x^2\right)\exp\left(-i\frac{2\pi}{\lambda z}np\Delta x\Delta\xi\right), \quad (7)$$

where $n\Delta x$ and $p\Delta\xi$ respectively denote the spatial coordinate in the CCD and reconstruction plane, and $N$ is the number of sampling points.

Direct implementation of Eq. (7) is a time-consuming process. Starting from Eq. (6), one can realize that efficient computational schemes can be designed to implement digital holographic reconstruction. This makes it possible to separate reconstruction methods into two main families: the Fourier based approaches [based on the use of a single fast Fourier transform (FFT)], well suited for imaging extended objects localized far from the CCD or CMOS sensor, and the convolution methods, computed by using two or three FFTs. These methods are well adapted for the reconstruction of holograms of small lateral dimensions, recorded near the imaging device. Alternative methods can be considered when an adjustable magnification or advanced filtering techniques are needed.

In the remainder of this section, we will detail the different computational approaches and apply these to the reconstruction of digital holograms.

### A. Single-FFT Method

Efficient implementation of Eq. (7) can be performed using the FFT algorithm [56,57]. In this case pixel pitches in both the reconstruction ($\Delta\xi$) and the CCD plane ($\Delta x$) are related by

$$\Delta\xi = \frac{\lambda z}{N\Delta x}. \quad (8)$$

Therefore, Eq. (7) can be rewritten as

$$E_{\mathrm{rec}}(p) = \frac{\exp\left(\frac{i2\pi}{\lambda}z\right)}{i\lambda z}\exp\left(i\frac{\pi\lambda z p^2}{N^2\Delta x^2}\right)\sum_{n=0}^{N-1}E(n) \times \exp\left(i\frac{\pi}{\lambda z}n^2\Delta x^2\right)\exp\left(-i2\pi\frac{np}{N}\right). \quad (9)$$

This relationship is therefore easily computed by

$$E_{\mathrm{rec}}(\xi) = \frac{\exp\left(\frac{i2\pi}{\lambda}z\right)}{i\lambda z}\exp\left(i\frac{\pi\lambda z p^2}{N^2\Delta x^2}\right) \times \mathcal{F}\left\{E(x)\exp\left(i\frac{\pi}{\lambda z}x^2\right)\right\}. \quad (10)$$

It should be noted that within this configuration, the ratio between the reconstructed horizon and the sensor array extension (which can be abusively denoted as the magnification of the reconstruction method) is closely linked to the reconstruction distance, i.e., $\gamma = \Delta\xi/\Delta x = \lambda z/(N\Delta x^2)$. In the remainder of this paper, the intrinsic magnification of the single-FFT implementation of the reconstruction integral will be denoted by $\gamma_0 = \lambda z/(N\Delta x^2)$.

### B. Convolution Based approaches

Holographic reconstruction can be viewed as a linear system. As matter of fact, Eq. (6) is the mathematical expression of the spatial convolution between the hologram and the Fresnel impulse response function $h_z$, which is defined by (omitting the multiplicative constant)

$$h_z(x) = \exp\left(i\frac{\pi}{\lambda z}x^2\right). \quad (11)$$

Convolution based approaches lead to unitary magnification, namely, $\Delta\xi = \Delta x$.

#### 1. *"Three-FFT Algorithm"*

Computation of the convolution product between the hologram and the holographic impulse response can

be efficiently implemented in Fourier domain. Using fast Fourier transform algorithms, Eq. (6) can be computed as

$$E_{\mathrm{rec}}(\xi) = \frac{\exp\left(\frac{i2\pi}{\lambda}z\right)}{i\lambda z}\mathcal{F}^{-1}[\mathcal{F}\{E(x)\} \times \mathcal{F}\{h_z(x)\}], \quad (12)$$

where $\mathcal{F}$ and $\mathcal{F}^{-1}$ respectively stand for the Fourier transform and its inverse.

### 2. *Angular Spectrum Propagation*

This method is based on the propagation of the angular spectrum of the hologram. The angular spectrum transfer function is given by [58]

$$H(u) \approx \exp\left[2i\frac{\pi z}{\lambda}\left(1 - \frac{1}{2}\lambda^2 u^2\right)\right], \quad (13)$$

where $u$ is the spatial frequency in Fourier domain. Using Eq. (13), hologram reconstruction can be performed:

$$E_{\mathrm{rec}}(\xi) = \frac{1}{i\lambda z}\mathcal{F}^{-1}[\mathcal{F}\{E(x)\} \times H(u)]. \quad (14)$$

## C. Algorithms with Adjustable Magnification

Neither the single-FFT approach nor the convolution based methods allow adjustment of the magnification of the reconstructed hologram. As a matter of fact, in single-FFT hologram processing, magnification depends on the recording wavelength and distance, whereas it remains constant using a convolution approach. In the latter case, the magnification is unitary ($\Delta\xi = \Delta x$). This aspect is illustrated by Fig. 2. Here, the evolution of the reconstructed horizon is represented with respect to the reconstruction distance. The solid lines are associated with the single-FFT reconstruction scheme, and the doted lines are the reconstruction horizon of the convolution based reconstruction approaches. It should be noted that for $z = N\Delta x^2/\lambda$ [this distance is determined by taking $\Delta x = \Delta\xi$ in Eq. (8)], single-FFT and convolution approaches exhibit the same magnification.

Working with an adjustable magnification algorithm is a great opportunity to make the reconstruction horizon independent from the hologram recording parameters. Domains such as multiwavelength holography benefit from this property [59,60].

Several approaches have been proposed to allow magnification adjustment. Ferraro *et al.* used zero-padding to control the reconstructed horizon and to make it independent from the reconstructed distance [61]. This method gives good results for multiwavelength hologram multiplexing but may, however, increase the computational load. Another way to adjust the magnification is to reconstruct the hologram with a two-step algorithm [62]. Each step consists of a single-FFT reconstruction. Letting $z$ be the reconstruction distance, the two steps (reconstruction at distances $z_1$ and $z_2$) are chosen such that $z = z_1 + z_2$. Here, the magnification is controlled by the choice of the intermediate reconstruction distance $z_1$. An optimization of this approach allows the authors of Ref. [63] to better match physical diffraction, thus obtaining high-fidelity reconstruction of magnified holograms. Control of reconstruction magnification, shift, and aberration compensation has also been proposed and realized using a digital lens with adjustable parameters in the reconstruction process [64].

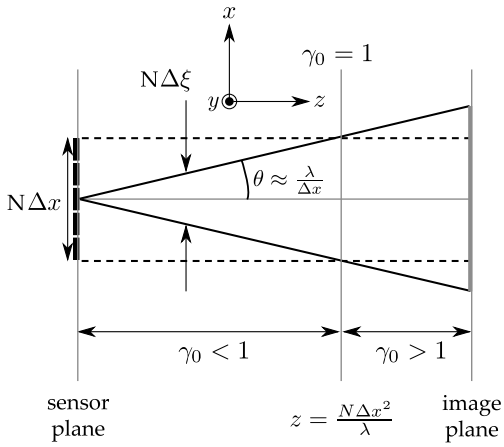


Fig. 2. Angular acceptance of digital holographic reconstruction process. Solid lines are associated with the single-FFT reconstruction, and dashed lines correspond to the convolution approaches.

In the following subsection, we will focus on two algorithms that allow adjustment of magnification in the reconstruction process and that are based either on the convolution [65] or the single-FFT [66] implementation of the Fresnel transform.

### 1. *Digital Quadratic Lens Method*

This method is based on the convolution approach [59,60]. Prior to reconstruction, the hologram is padded to the desired horizon and then multiplied by a digital spherical wavefront acting as a quadratic lens, which is defined by

$$\mathcal{L}(x) = \exp\left(-i\frac{\pi}{\lambda R_c}x^2\right), \quad (15)$$

where $R_c$ denotes the curvature radius of $\mathcal{L}$. This curvature radius can be defined in terms of system magnification such that

$$R_c = \frac{\gamma z}{\gamma - 1}. \quad (16)$$

Here, $\gamma$ is the ratio between the CCD horizon (of the padded hologram) and the object's physical extent. Working with a spherical reconstruction wavefront modifies the physical reconstruction distance $z$ to $z' = \gamma z$. Thus, hologram reconstruction can be realized by computing the following relation:

$$E_{\mathrm{rec}}(\xi) = \frac{\exp\left(\frac{i2\pi}{\lambda}z'\right)}{i\lambda z'}\mathcal{F}^{-1}[\mathcal{F}\{E(x)\mathcal{L}(x)\} \times \mathcal{F}\{h_{z'}(x)\}], \tag{17}$$

when working within a "three-FFT" scheme, or

$$E_{\mathrm{rec}}(\xi) = \frac{\exp\left(\frac{i2\pi}{\lambda}z'\right)}{i\lambda z'}\mathcal{F}^{-1}[\mathcal{F}\{E(x)\mathcal{L}(x)\} \times H(u)], \tag{18}$$

when angular spectrum propagation is considered. An alternative method, based on this formalism associated with a spatial filtering of the single-FFT reconstructed hologram, allows the reconstruction of the local object field with an adjustable magnification [65]. This method makes it possible to limit the effect of the reference beam distortions. However, one more FFT (two, when the angular spectrum implementation is considered) is needed to deal with the filtering step.

### 2. *Fresnel–Bluestein Transform*

This approach is based on a "clever" expansion of Eq. (9) [66]. In the kernel of the Fourier transform, the product $2np$ is rewritten as $2np = n^2 + p^2 - (p-n)^2$ [67], such that the discrete Fresnel transform can be expressed by

$$\begin{aligned} E_{\mathrm{rec}}(p) = {} & \frac{\exp\left(\frac{i2\pi}{\lambda}z\right)}{i\lambda z}\exp\left[-\frac{i\pi}{\lambda z}\Delta\xi(\Delta x - \Delta\xi)p^2\right] \\ & \times \sum_{n=0}^{N} E(n)\exp\left[\frac{i\pi}{\lambda z}\Delta x(\Delta x - \Delta\xi)n^2\right] \\ & \times \exp\left[\frac{i\pi}{\lambda z}\Delta x\Delta\xi(p-n)^2\right]. \end{aligned} \tag{19}$$

Let $\gamma = \Delta\xi/\Delta x$ be the magnification of the reconstruction. Therefore, Eq. (19) can be rewritten as

$$\begin{aligned} E_{\mathrm{rec}}(p) = {} & \frac{\exp\left(\frac{i2\pi}{\lambda}z\right)}{i\lambda z}\exp\left[-\frac{i\pi}{\lambda z}\gamma(1-\gamma)\Delta x^2 p^2\right] \\ & \times \sum_{n=0}^{N} E(n)\exp\left[\frac{i\pi}{\lambda z}(1-\gamma)n^2\Delta x^2\right] \\ & \times \exp\left[\frac{i\pi}{\lambda z}\gamma(p-n)^2\Delta x^2\right]. \end{aligned} \tag{20}$$

It should be noted that the magnification $\gamma$ is independent of the hologram recording parameters and can be adjusted at will. With this formulation, Eq. (20) is the spatial convolution product of two functions $f$ and $g$, defined by

$$f(n) = E(n)\exp\left[i\frac{\pi}{\lambda z}(1-\gamma)n^2\Delta x^2\right] \tag{21}$$

and

$$g(n) = \exp\left(i\frac{\pi}{\lambda z}\gamma n^2\Delta x^2\right). \tag{22}$$

The Fresnel–Bluestein reconstruction algorithm can, therefore, be summarized as

$$\begin{aligned} E_{\mathrm{rec}}(\xi) = {} & \frac{\exp\left(\frac{i2\pi}{\lambda}z\right)}{i\lambda z}\exp\left[-\frac{i\pi}{\lambda z}\gamma(1-\gamma)\Delta x^2 p^2\right] \\ & \times \mathcal{F}^{-1}[\mathcal{F}\{f(x)\} \times \mathcal{F}\{g(x)\}]. \end{aligned} \tag{23}$$

Adjustable magnification rendering with the quadratic lens method and the Fresnel–Bluestein algorithm yield the same results. Let $\gamma_0$ be the intrinsic magnification of the single-FFT reconstruction scheme. Hologram rendering of a United States Air Force (USAF) resolution target sector with 228 line pairs.mm$^{-1}$ spatial frequency at element (7-6), with both methods at magnification $\gamma = 0.8, 1, 2.5 \times \gamma_0$, is reported in Fig. 3. Although these two methods are based on different formalisms (single-FFT formalism and convolution based approach), it is here made obvious that both methods lead to the same results.

### 3. *Aliases and Replicas*

Adjustable magnification algorithms make it possible either to zoom over details in reconstructed images or to reconstruct objects whose dimensions are greater than that of the recording device. However, care must be taken. As a matter of fact, working with reconstruction horizons smaller than the object's physical extent may cause aliases in the reconstruction plane, whereas replicas may appear in the opposite situation. In other words, considering $\gamma_0 = \lambda z/(N\Delta x^2)$ the intrinsic magnification of the single-FFT based Fresnel transform implementation,

$$\gamma < \gamma_0 \tag{24}$$

will lead to replicas in the reconstructed image, whereas choosing

$$\gamma > \gamma_0 \tag{25}$$

will generate aliases. This aspect is illustrated by Figs. 4(a) and 4(c). A hologram of the object was reconstructed using the adjustable magnification algorithm proposed by Restrepo and Garcia-Sucerquia [66] (the results would have been the same if the quadratic lens algorithm was considered). The reconstruction with the single-FFT algorithm ($\gamma = \gamma_0$) is proposed in Figs. 4(b) and 4(e). It should be noted that replicas can be seen in Fig. 4(a) (here $\gamma < \gamma_0$), and aliases appear in Fig. 4(c) (for $\gamma > \gamma_0$). These unwanted effects degrade the reconstruction quality and must be avoided.

To limit the aliasing effect, when $\gamma > \gamma_0$, Hennelly *et al.* proposed a filtering scheme, which is presented

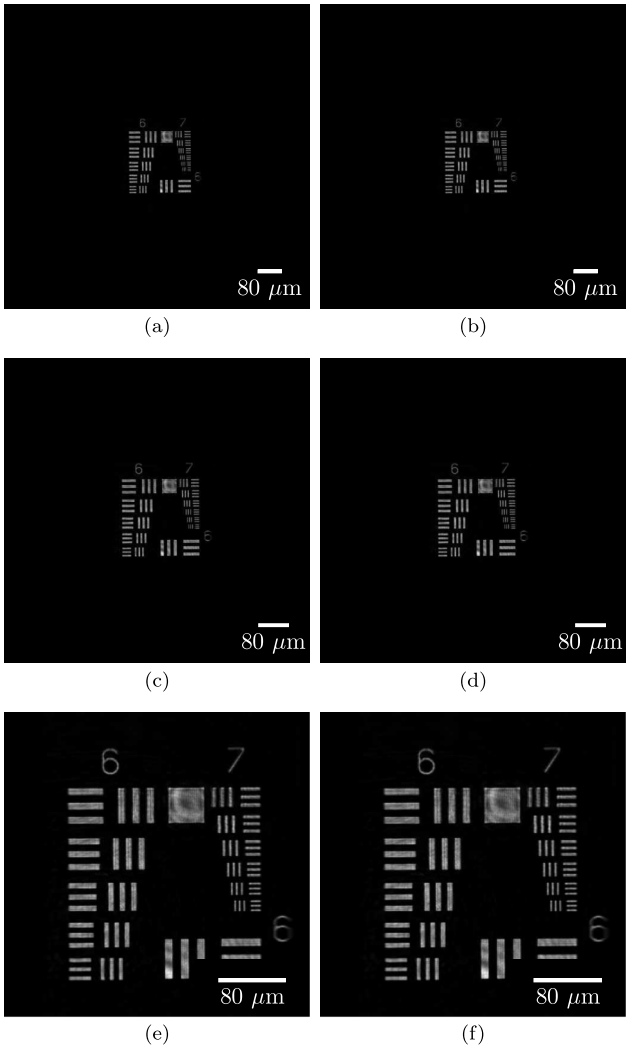


Fig. 3. Reconstruction of a hologram for $\gamma = 0.8, 1, 2.5 \times \gamma_0$. (a), (c), (e) Quadratic lens method, (b), (d), (f) Fresnel–Bluestein method.

in Fig. 5(a) [68]. Prior to being reconstructed, the hologram is multiplied by a chirp function defined as

$$\mathcal{C}(x) = \exp\left(i\frac{\pi}{\lambda z}x^2\right). \tag{26}$$

The resulting chirp-multiplied hologram is then low-pass filtered and finally multiplied by $\mathcal{C}^*$, which is the complex conjugate of $\mathcal{C}$. The size of the filtering window is chosen so as to match the physical extent of the reconstruction horizon at distance $z$. It is therefore possible to reconstruct the hologram using an adjustable magnification algorithm. Benefits of this filtering approach are illustrated by Figs. 4(c) and 4(f). Alias artifacts are completely removed, thus giving a high-contrast image of the reconstructed objects.

When $\gamma < \gamma_0$, replicas can be seen on the reconstructed image. Their removal can be performed by the procedure illustrated in Fig. 5(b). The reconstructed hologram is cropped in order to keep the $(\gamma_0/\gamma)N$ pixels associated with the original object. This selection is then zero-padded to the original size of the hologram. As can be seen from Figs. 4(a) and 4(d), replicas are completely removed.

### D. Fresnelet Decomposition

Fresnelet decomposition was initially proposed by Liebling *et al.* for the reconstruction and processing of digital holograms [69]. This multiresolution scheme finds application in a wide variety of domains such as data compression [70,71], nonlinear filtering [72], and wavefront retrieving [73] and can be considered in autofocusing procedures [74]. Fresnelet reconstruction of a hologram consists of its decomposition on the basis of Fresnel-transformed wavelets.

Liebling proposed the use of B-splines, which can be defined as [69]

$$\beta^n(x) = \underbrace{\beta^0 * \ldots * \beta^0}_{n+1}(x), \tag{27}$$

where $\beta^0$ is given by

$$\beta^0(x) = \begin{cases} 1, & 0 < x < 1 \\ \frac{1}{2}, & x = 0 \text{ or } x = 1 \\ 0, & \text{otherwise} \end{cases}, \tag{28}$$

and the $*$ symbol denotes the convolution product. As shown by Unser *et al.*, the B-spline fulfills all the mathematical requirements to be used for multiresolution analysis of $L_2(\mathbb{R})$ [75], especially the two-scale relation:

$$\beta^n\left(\frac{x}{2}\right) = \sum_{k\in\mathbb{Z}} h(k)\beta^n(x-k). \tag{29}$$

Here $h(k) = \frac{1}{2^n}\binom{n+1}{k}$ is the binomial filter.

A B-spline can be used to generate a semiorthogonal wavelet function basis of $L_2(\mathbb{R})$ denoted by $\psi^n_{j,k}$ and defined as

$$\{\psi^n_{j,k} = 2^{\frac{-j}{2}}\psi^n(2^{-j}x-k)\}_{j,k\in\mathbb{Z}}, \tag{30}$$

where

$$\psi^n\left(\frac{x}{2}\right) = \sum_{k\in\mathbb{Z}} g(k)\beta^n(x-k). \tag{31}$$

The filter $g(k)$ is the quadrature mirror filter of $h(k)$. Fresnelet basis can be calculated simply by taking the Fresnel transform of the B-spline basis. Fresnelet bases are therefore defined by

$$\{\tilde{\psi}^n_{j,k} = 2^{\frac{-j}{2}}\tilde{\psi}^n(2^{-j}x-k)\}_{j,k\in\mathbb{Z}}, \tag{32}$$

with

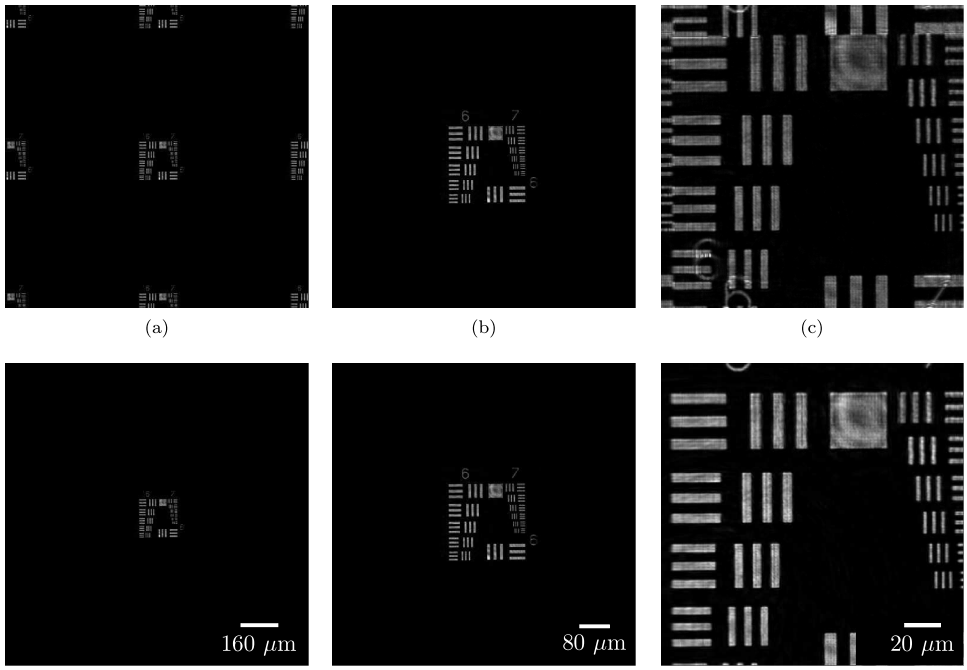


(a) (b) (c)

(d) (e) (f)

Fig. 4. Illustrations of alias and replica phenomena. (a) Reconstruction with $\gamma = 0.5 \times \gamma_0$, (c) reconstruction with $\gamma = 4 \times \gamma_0$, (d) same as (a) with replica removal, (f) same as (c) with alias filtering, (b), (e) reconstruction with $\gamma = \gamma_0$.

$$\tilde{\psi}^n\left(\frac{x}{2}\right) = \sum_{k\in\mathbb{Z}} g(k)\tilde{\beta}^n(x-k), \tag{33}$$

and

$$\tilde{\beta}^n\left(\frac{x}{2}\right) = \sum_{k\in\mathbb{Z}} h(k)\tilde{\beta}^n(x-k). \tag{34}$$

Here $\tilde{\cdot}$ is associated with the Fresnel transform.

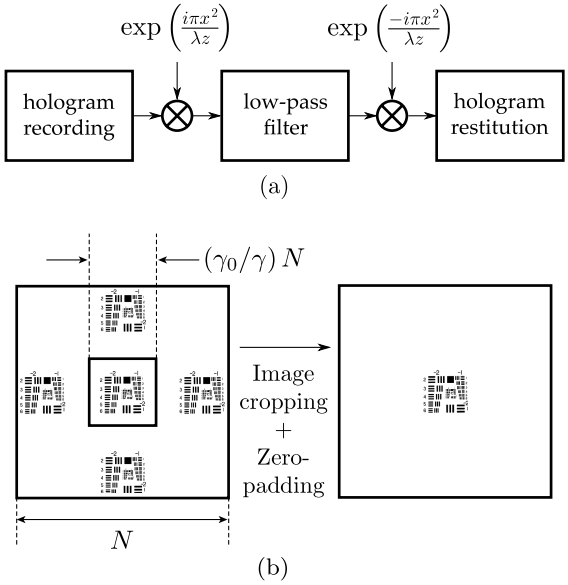


Fig. 5. (a) Synoptics of the antialias procedure, (b) replica removal scheme.

It should be noted that the computation method chosen for the Fresnel transform will affect the Fresnelet transform results. As a matter of fact, Fresnelet transform properties will be the same as those of the chosen Fresnel computation scheme (e.g., adjustable or unitary magnification).

## 4. Application

In this section, reconstruction of experimental holograms is performed according to the methods reported in Section 3. Holograms are recorded according to the experimental setup of Fig. 6. Here, off-axis interference between the reference and object beams are recorded on a $2048 \times 2048$ pixel CCD sensor with a $\Delta x = 7.4\,\mu$m pixel pitch. The object consists of an inverted USAF target illuminated with a green laser ($\lambda = 532\,$nm). The USAF target is positioned at three different distances, $z_i$, from the sensor, chosen such that $\Delta\xi < \Delta x$, $\Delta\xi = \Delta x$, and $\Delta\xi > \Delta x$, where $\Delta\xi$ and $\Delta x$ denote the size of the reconstruction and of the CCD sensor, respectively. Experimental reconstructions are presented hereafter.

### A. Classical Reconstruction Methods

In this section, holograms recorded at $z_i$ such that $\Delta\xi < \Delta x$, $\Delta\xi = \Delta x$, and $\Delta\xi > \Delta x$, are reconstructed using single-FFT, angular spectrum propagation, and three-FFT methods. Images of the reconstructed objects are proposed in Fig. 7. This figure consists of a two-entry table. In each row, the holograms reconstructed when $\Delta\xi < \Delta x$, $\Delta\xi = \Delta x$, and $\Delta\xi > \Delta x$ are depicted. Each column is associated with the chosen reconstruction method: single-FFT, angular spectrum propagation, and three-FFT. It is noticeable

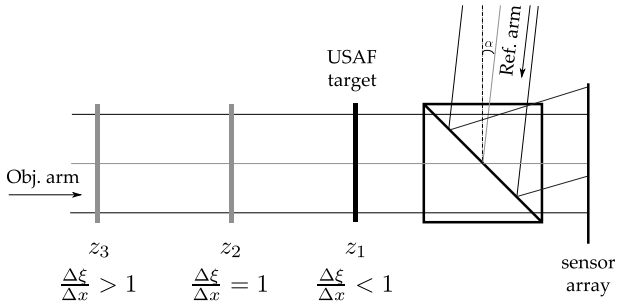


Fig. 6. Experimental procedure for the holographic reconstruction benchmarking.

that in most cases reconstruction results depend on the method chosen. In the following section, results obtained are detailed row by row.

### 1. *Reconstruction for* $\Delta\xi < \Delta x$

1. Single-FFT

As seen on Fig. 7, aliases are present in the reconstructed image of the object. This is due to the fact that the single-FFT implementation of the Fresnel transform results in a magnified image of the original object. Thus, the reconstructed object extends over the limits of the CCD sensor.

2. Angular Spectrum

As far as $\Delta\xi < \Delta x$, the reconstructed object is well embedded within the CCD sensor horizon. The angular spectrum method is therefore well suited for reconstruction of holograms recorded near the CCD sensor.

3. Three-FFT

The reconstructed image of the object is embedded within the CCD sensor. However, replicas can be noticed from the reconstructed hologram. This is due to the fact that when the reconstruction distance $z < N\Delta x/\lambda$, the impulse response $h_z$ is ill-sampled; in this situation, the sampling theorem is not verified [76].

### 2. *Reconstruction for* $\Delta\xi = \Delta x$

It can be noted that for $\Delta\xi = \Delta x$, the three reconstruction methods considered give the same results. As a matter of fact, in this situation, the reconstructed horizon perfectly matches the sensor array extent. In other words, intrinsic magnification of

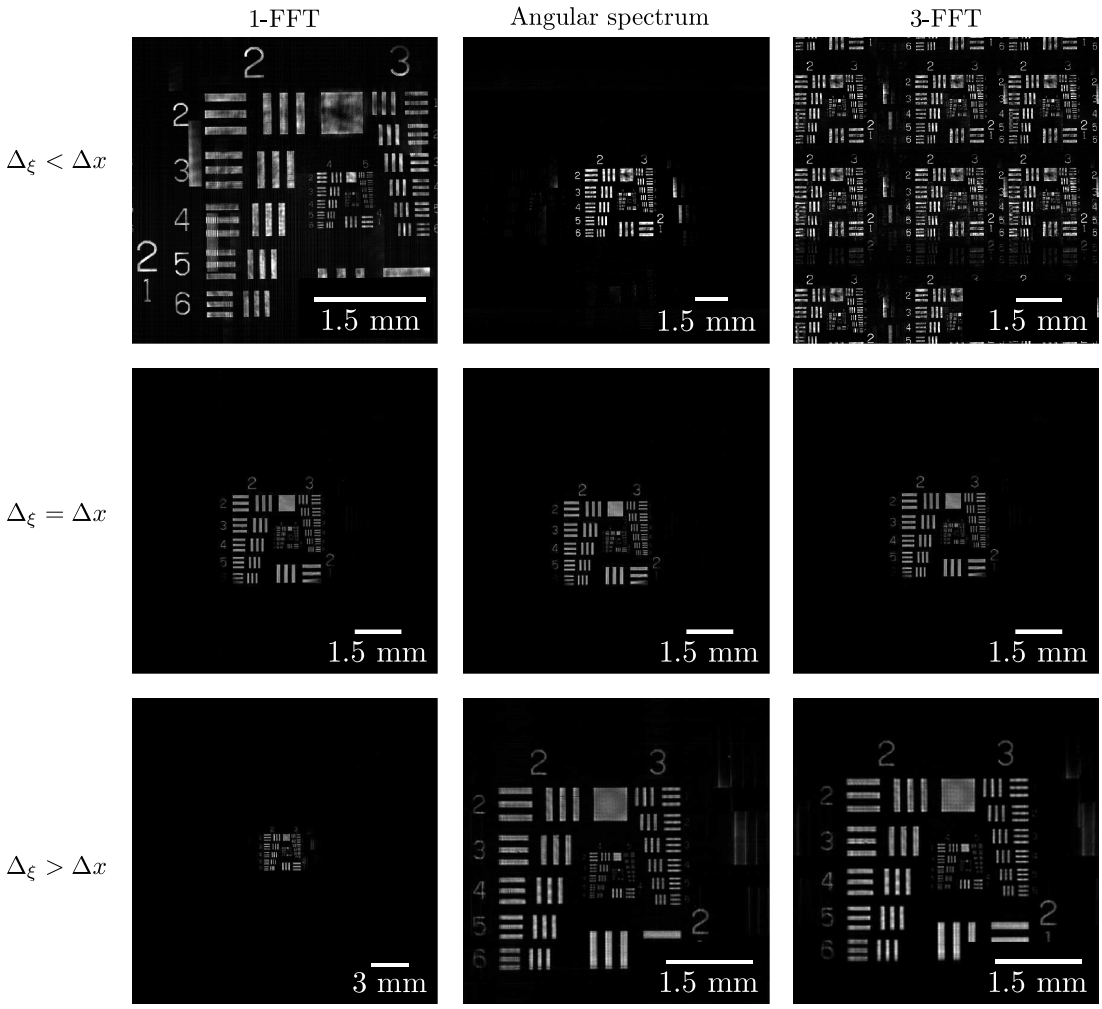


Fig. 7. Holographic reconstructions of the USAF target located at different distances.

single-FFT Fresnel implementation is the same as that of convolution approaches.

### 3. *Reconstruction for* $\Delta\xi > \Delta x$

1. Single-FFT

As far as the object extent is bigger than the sensor array dimensions, the single-FFT implementation of the Fresnel transform is appropriate for hologram reconstruction.

2. Angular Spectrum and Three-FFT

The fact that these approaches exhibit unitary magnification is limiting when dealing with an object located far from the sensor. As a matter of fact, it can be realized from Fig. 7 that aliases occur in the reconstructed image of the hologram.

Classical reconstruction methods have been applied to experimental holograms recorded at various distances from the sensor array. It can be noted that each method is valid only within a limited range of distances. In the next section, we will give a few words about Fresnelet decomposition and show that its reconstruction properties can be modified to match each reconstruction method.

## B. Fresnelets

As presented in Section 3.D, Fresnelet decomposition is similar to a multiscale-wavelet decomposition on a Fresnel-transformed base. One appealing feature of this decomposition is that the result of the Fresnelet reconstruction depends on the method chosen to compute the Fresnel transform of the wavelet base.

To illustrate this point, Fresnelet reconstruction of the hologram recorded for $\Delta\xi > \Delta x$ is performed. In this situation, the single-FFT method gives good results, whereas the three-FFT reconstruction produces alises. Here, the fresnelet bases are calculated with the single-FFT and the three-FFT method according to Eqs. (33) and (34). Decompositions of the test hologram on the two calculated fresnelet bases are proposed in Figs. 8(a) and 8(b), respectively. It should be noticed that the computation scheme chosen strongly affects the calculated coefficients. Therefore, properties of the fresnelet decomposition reconstruction depend on the method chosen to calculate the fresnelet base functions. This aspect is pointed out by Figs. 8(c) and 8(d). Here, hologram reconstruction from the Fresnelet coefficients depicted in Figs. 8(a) and 8(b) is realized. These reconstructions are similar to the one obtained with classical methods (see $\Delta\xi > \Delta x$ in Fig. 7 for comparison). Thus, for $\Delta\xi > \Delta x$, the single-FFT method will be more reliable than the three-FFT scheme.

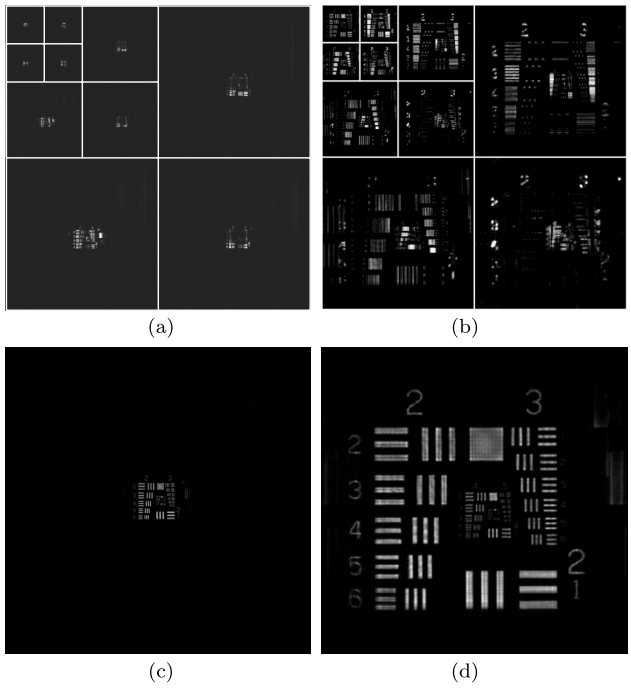


Fig. 8. Fresnelet decomposition of the hologram recorded for $\Delta\xi > \Delta x$. (a) Fresnelet coefficients computed within the single-FFT scheme, (b) Fresnelet coefficients computed within the three-FFT scheme, (c) hologram reconstruction from (a), (d) hologram reconstruction from (b).

## 5. Conclusion

We have proposed an overview of holographic reconstruction methods with application to off-axis intensity hologram treatment. Intrinsic properties and limitations of classical methods have been investigated, and applicability ranges have been stated with the reconstruction of experimental holograms. It can be noted that the choice of the reconstruction method will be driven by the hologram recording conditions. For instance, when dealing with far and extended objects, the single-FFT algorithm will be the most appropriate, whereas convolution approaches will be suited for the reconstruction of small objects located near the sensor array. Adjustable magnification methods have been presented and can be viewed as a way to overcome limitations of the classical reconstruction schemes and allow the reconstruction result to be independent from the chosen scheme. Nevertheless, care must be taken in order to limit aliases and replicas when working with high or low magnification. Finally, Fresnelet reconstruction of the holograms has been performed using the fact that the Fresnelet decomposition base depends on the method chosen to compute the Fresnel transform. This method can be considered for filtering or image compression when computational load is not a critical issue.

This work was funded by Fondation Pierre-Gilles de Gennes (grant FPGG014), Agence Nationale de la Recherche (grant ANR-09-JCJC-0113), and Région Île-de-France (C'Nano grant).

## References

1. D. Gabor, "A new microscopic principle," Nature **161**, 777–778 (1948).
2. D. Gabor, "Microscopy by reconstructed wave-fronts," Proc. R. Soc. Lond. A **197**, 454–487 (1949).
3. E. N. Leith and J. Upatnieks, "Reconstructed wavefronts and communication theory," J. Opt. Soc. Am. **52**, 1123–1130 (1962).

4. J. W. Goodman and R. W. Lawrence, "Digital image formation from electronically detected holograms," Appl. Phys. Lett. **11**, 77–79 (1967).
5. M. A. Kronrod, N. S. Merzlyakov, and L. P. Yaroslavsky, "Reconstruction of holograms with a computer," Sov. Phys. Tech. Phys. **17**, 419–420 (1972).
6. L. P. Yaroslvsky and N. S. Merzlyakov, *Methods of Digital Holography* (Springer, 1980).
7. L. Onural and P. D. Scott, "Digital recording of in-line holograms," Opt. Eng. **26**, 1124–1132 (1987).
8. G. Liu and P. D. Scott, "Phase retrieval and twin-image elimination for in-line Fresnel holograms," J. Opt. Soc. Am. A **4**, 159–165 (1987).
9. J. R. Fienup, "Phase retrieval algorithms, a comparison," Appl. Opt. **21**, 2758–2769 (1982).
10. L. Onural and M. T. Ozgen, "Extraction of three-dimensional object-location information directly from in-line holograms using Wigner analysis," J. Opt. Soc. Am. A **9**, 252–260 (1992).
11. U. Schnars and W. Jüptner, "Direct recording of holograms by a CCD target and numerical reconstruction," Appl. Opt. **33**, 179–181 (1994).
12. A. Lozano, J. Kostas, and J. Soria, "Use of holography in particle image velocimetry measurements of a swirling flow," Exp. Fluids **27**, 251–261 (1999).
13. H. Meng, G. Pan, Y. Pu, and S. H. Woodward, "Holographic particle image velocimetry: from film to digital recording," Meas. Sci. Technol. **15**, 673–685 (2004).
14. Y. Pu and H. Meng, "Four-dimensional dynamic flow measurement by holographic particle image velocimetry," Appl. Opt. **44**, 7697–7708 (2005).
15. F. Dubois, N. Callens, C. Yourassowsky, M. Hoyos, P. Kurowski, and O. Monnom, "Digital holographic microscopy with reduced spatial coherence for three-dimensional particle flow analysis," Appl. Opt. **45**, 864–871 (2006).
16. M. Atlan and M. Gross, "Laser Doppler imaging, revisited," Rev. Sci. Instrum. **77**, 116103 (2006).
17. J-M. Desse, P. Picart, and P. Tankam, "Digital three-color holographic interferometry for flow analysis," Opt. Express **16**, 5471–5480 (2008).
18. N. Verrier, S. Coëtmellec, M. Brunel, and D. Lebrun, "Digital in-line holography in thick optical systems: application to visualization in pipes," Appl. Opt. **47**, 4147–4157 (2008).
19. N. Verrier, S. Coëtmellec, M. Brunel, and D. Lebrun, "Determination of 3D-region of interest using digital in-line holography with astigmatic Gaussian beams," J. Europ. Opt. Soc. Rapid Publ. **4**, 09038 (2009).
20. N. Verrier, C. Remacha, M. Brunel, D. Lebrun, and S. Coëtmellec, "Micropipe flow visualization using digital in-line holographic microscopy," Opt. Express **18**, 7807–7819 (2010).
21. S. Schedin, G. Pedrini, and H. J. Tiziani, "Pulsed digital holography for deformation measurements on biological tissues," Appl. Opt. **39**, 2853–2857 (2000).
22. M. K. Kim, "Tomographic three-dimensional imaging of a biological specimen using wavelength-scanning digital interference holography," Opt. Express **7**, 305–310 (2000).
23. F. Charrière, N. Pavillon, T. Colomb, C. Depeursinge, T. J. Heger, E. A. D. Mitchell, P. Marquet, and B. Rappaz, "Living specimen tomography by digital holographic microscopy: morphometry of testate amoeba," Opt. Express **14**, 7005–7013 (2006).
24. W. Xu, M. H. Jericho, I. A. Meinertzhagen, and H. J. Kreuzer, "Digital in-line holography for biological applications," Proc. Natl. Acad. Sci. USA **98**, 11301–11305 (2001).
25. B. Kemper and G. von Bally, "Digital holographic microscopy for live cell applications and technical inspection," Appl. Opt. **47**, A52–A61 (2008).
26. M. Simonutti, M. Paques, J. A. Sahel, M. Gross, B. Samson, C. Magnain, and M. Atlan, "Holographic laser Doppler ophthalmoscopy," Opt. Lett. **35**, 1941–1943 (2010).
27. R. L. Powell and K. A. Stetson, "Interferometric vibration analysis by wavefront reconstruction," J. Opt. Soc. Am. **55**, 1593–1597 (1965).
28. C. C. Aleksoff, "Temporally modulated holography," Appl. Opt. **10**, 1329–1341 (1971).
29. F. Zhang, J. D. R. Valera, I. Yamaguchi, M. Yokota, and G. Mills, "Vibration analysis by phase shifting digital holography," Opt. Rev. **11**, 297–299 (2004).
30. U. Iemma, L. Morino, and M. Diez, "Digital holography and Karhunen-Loève decomposition for the modal analysis of two-dimensional vibrating structures," J. Sound Vib. **291**, 107–131 (2006).
31. P. Picart, J. Leval, D. Mounier, and S. Gougeon, "Some opportunities for vibration analysis with time averaging in digital Fresnel holography," Appl. Opt. **44**, 337–343 (2005).
32. J. Leval, P. Picart, J-P. Boileau, and J-C. Pascal, "Full-field vibrometry with digital Fresnel holography," Appl. Opt. **44**, 5763–5772 (2005).
33. D. Borza, "Mechanical vibration measurement by high-resolution time-averaged digital holography," Meas. Sci. Technol. **16**, 1853–1864 (2005).
34. A. Asundi and V. R. Singh, "Time-averaged in-line digital holographic interferometry for vibration analysis," Appl. Opt. **45**, 2391–2395 (2006).
35. F. Joud, F. Lanoë, M. Atlan, J. Hare, and M. Gross, "Imaging a vibrating object by sideband digital holography," Opt. Express **17**, 2774–2779 (2009).
36. I. Yamaguchi, K. Yamamoto, G. A. Mills, and M. Yokota, "Image reconstruction only by phase data in phase-shifting holography," Appl. Opt. **45**, 975–983 (2006).
37. K. Matsushima, "Shifted angular spectrum method for off-axis numerical propagation," Opt. Express **18**, 18453–18463 (2010).
38. D. Lebrun, A. Benkouider, S. Coëtmellec, and M. Malek, "Particle field digital holographic reconstruction in arbitrary tilted planes," Opt. Express **11**, 224–229 (2003).
39. S. De Nicola, A. Finizio, G. Pierattini, P. Ferraro, and D. Alfieri, "Angular spectrum method with correction of anamorphism for numerical reconstruction on tilted planes," Opt. Express **13**, 9935–9940 (2005).
40. N. Verrier, S. Coëtmellec, M. Brunel, D. Lebrun, and A. J. E. M. Janssen, "Digital in-line holography with an elliptical, astigmatic, Gaussian beam: wide angle reconstruction," J. Opt. Soc. Am. A **25**, 1459–1466 (2008).
41. F. Soulez, L. Denis, C. Fournier, E. Thiébaut, and C. Goepfert, "Inverse-problem approach for particle digital holography: accurate location based on local optimization," J. Opt. Soc. Am. A **24**, 1164–1171 (2007).
42. F. Soulez, L. Denis, E. Thiébaut, C. Fournier, and C. Goepfert, "Inverse-problem approach in particle digital holography: out-of-field particle detection made possible," J. Opt. Soc. Am. A **24**, 3708–3716 (2007).
43. L. Denis, D. Lorenz, E. Thiébaut, C. Fournier, and D. Trede, "Inline hologram reconstruction with sparsity constraints," Opt. Lett. **34**, 3475–3477 (2009).
44. M. Marim, E. Angelini, J-C. Olivo-Marin, and M. Atlan, "Off-axis compressed holographic microscopy in low-light conditions," Opt. Lett. **36**, 79–81 (2011).
45. T. Shimobaba, Y. Sato, J. Miura, M. Takenouchi, and T. Ito, "Real-time digital holographic microscopy using the graphic processing unit," Opt. Express **16**, 11776–11781 (2008).
46. L. Ahrenberg, A. J. Page, B. M. Hennelly, J. B. McDonald, and T. J. Naughton, "Using commodity graphics hardware

for real-time digital hologram view-reconstruction," IEEE J. Display Technol. **5**, 111–119 (2009).
47. T. Shimobaba, N. Masuda, Y. Ichihashi, and T. Ito, "Real-time digital holographic microscopy observable in multi-view and multi-resolution," J. Opt. **12**, 065402 (2010).
48. B. Samson, F. Verpillat, M. Gross, and M. Atlan, "Video-rate wide-field laser vibrometry by heterodyne holography," Opt. Lett. **36**, 1449–1451 (2011).
49. I. Yamaguchi and T. Zhang, "Phase-shifting digital holography," Opt. Lett. **22**, 1268–1270 (1997).
50. M. Atlan, M. Gross, and E. Absil, "Accurate phase-shifting digital interferometry," Opt. Lett. **32**, 1456–1458 (2007).
51. J. W. Goodman, *Introduction to Fourier Optics*, 3rd ed. (Roberts, 2005).
52. E. N. Leith and J. Upatnieks, "Wavefront reconstruction with continuous-tone objects," J. Opt. Soc. Am. **53**, 1377–1381 (1963).
53. E. Cuche, P. Marquet, and C. Depeursinge, "Spatial filtering for zero-order and twin-image elimination in digital off-axis holography," Appl. Opt. **39**, 4070–4075 (2000).
54. I. Yamaguchi, J. Kato, S. Ohta, and J. Mizuno, "Image formation in phase-shifting digital holography and applications to microscopy," Appl. Opt. **40**, 6177–6186 (2001).
55. M. Born and E. Wolf, *Principles of Optics*, 7th ed. (Cambridge University, 1999).
56. J. W. Cooley and J. W. Tukey, "An algorithm for the machine computation of complex Fourier series," Math. Comput. **19**, 297–301 (1965).
57. U. Schnars and W. Jüptner, "Digital recording and numerical reconstruction of holograms," Meas. Sci. Technol. **13**, R85–R101 (2002).
58. L. Yu and M. K. Kim, "Wavelength-scanning digital interference holography for tomographic three-dimensional imaging by use of the angular spectrum method," Opt. Lett. **30**, 2092–2094 (2005).
59. J. Li, P. Tankam, Z. Peng, and P. Picart, "Digital holographic reconstruction of large object using a convolution approach and adjustable magnification," Opt. Lett. **34**, 572–574 (2009).
60. P. Picart, P. Tankam, D. Mounier, Z-j. Peng, and J. Li, "Spatial bandwidth extended reconstruction for digital color Fresnel holograms," Opt. Express **17**, 9145–9156 (2009).
61. P. Ferraro, S. De Nicola, G. Coppola, A. Finizio, D. Alfieri, and G. Pierattini, "Controlling image size as a function of distance and wavelength in Fresnel-transform reconstruction of digital holograms," Opt. Lett. **29**, 854–856 (2004).
62. F. Zhang, I. Yamaguchi, and L. P. Yaroslavsky, "Algorithm for reconstruction of digital holograms with adjustable magnification," Opt. Lett. **29**, 1668–1670 (2004).
63. D. Wang, J. Zhao, F. Zhang, G. Pedrini, and W. Osten, "High-fidelity numerical realization of multiple-step Fresnel propagation for the reconstruction of digital holograms," Appl. Opt. **47**, D12–D20 (2008).
64. T. Colomb, F. Montfort, J. Kühn, N. Aspert, E. Cuche, A. Marian, F. Charrière, S. Bourquin, P. Marquet, and C. Depeursinge, "Numerical parametric lens for shifting, magnification, and complete aberration compensation in digital holographic microscopy," J. Opt. Soc. Am. A **23**, 3177–3190 (2006).
65. J. Li, Z. Peng, P. Tankam, Q. Song, and P. Picart, "Digital holographic reconstruction of a local object field using an adjustable magnification," J. Opt. Soc. Am. A **28**, 1291–1296 (2011).
66. J. F. Restrepo and J. Garcia-Sucerquia, "Magnified reconstruction of digitally recorded holograms by Fresnel-Bluestein transform," Appl. Opt. **49**, 6430–6435 (2010).
67. L. Bleustein, "Linear filtering approach to the computation of the discrete Fourier transform," IEEE Trans. Audio Electroacoust. **18**, 451–455 (1970).
68. B. Hennelly, D. Kelly, N. Pandey, and D. Monaghan, "Zooming algorithms for digital holography," J. Phys. Conf. Ser. **206**, 012027 (2010).
69. M. Liebling, T. Blu, and M. Unser, "Fresnelet: new multiresolution wavelet bases for digital holography," IEEE Trans. Image Process. **12**, 29–43 (2003).
70. E. Darakis and J. J. Soraghan, "Use of Fresnelets for phase-shift digital hologram compression," IEEE Trans. Image Process. **15**, 3804–3811 (2006).
71. E. Darakis, T. J. Naughton, and J. J. Soraghan, "Compression defect in different reconstructions from phase-shifting digital holographic data," Appl. Opt. **46**, 4579–4586 (2007).
72. M. Liebling, T. Blu, and M. Unser, "Non-linear Fresnelet approximation for interference term suppression in digital holography," Proc. SPIE **5207**, 553–559 (2003).
73. M. Liebling, T. Blu, and M. Unser, "Complex-wave retrieval from a single off-axis hologram," J. Opt. Soc. Am. A **21**, 367–377 (2004).
74. M. Liebling and M. Unser, "Autofocus for digital Fresnel holograms by use of a Fresnelet-sparsity criterion," J. Opt. Soc. Am. A **21**, 2424–2430 (2004).
75. M. Unser, A. Aldroubi, and M. Eden, "A family of polynomial spline wavelet transforms," Signal Process. **30**, 141–162 (1993).
76. L. Onural, "Sampling of the diffraction field," Appl. Opt. **39**, 5929–5935 (2000).